Turbulence level effects on conventional reflectometry using 2D full-wave simulations[a)]

J. Vicente,[1,b)] F. da Silva,[1] S. Heuraux,[2] G.D. Conway,[3] C. Silva,[1] and T. Ribeiro[3]

[1]*Instituto de Plasmas e Fusão Nuclear, Instituto Superior Técnico, Universidade de Lisboa, 1049-001 Lisboa, Portugal*
[2]*Institut Jean Lamour, UMR 7198 CNRS-University of Lorraine, F-54506 Vandoeuvre, France*
[3]*Max-Planck-Institut für Plasmaphysik, 85748 Garching, Germany*

Numerical simulations are critical in improving the capabilities of microwave diagnostics. In this work, the 2D finite-difference time-domain full-wave code REFMUL was applied to broadband turbulent plasmas using the conventional reflectometry set-up. Simulations were performed with O-mode waves, fixed frequency probing and I/Q detection. The plasma density, determining O-mode propagation, was modeled as the sum of a slab background plasma with a fluctuating component following a Kolgomorov-like amplitude k-spectrum. The density turbulence level $\delta n_e/n_e$ was scanned over several orders of magnitude for simulated plasma flows of constant plasma velocity in either the radial or the poloidal direction. Simulations show trends, such as spectral broadening of the complex $A(t)e^{i\varphi(t)}$ signals and increasing fluctuations in $A(t)$ and $\varphi(t)$ with increasing $\delta n_e/n_e$, that are similar for both plasma flow directions. These, together with possibilities to reconstruct poloidal wavenumber spectrum are discussed in view to extending the measuring capabilities. The onset of non-linear effects associated with phase runaway, as previously observed with other 1D and 2D codes, as well as radial Doppler effects are also observed and discussed.

I. INTRODUCTION

Full-wave simulations have been instrumental in understanding reflectometry measurements and plasma-wave interactions, such as Bragg backscattering or forward scattering[1]. In this work, the response of ordinary wave polarization (O-mode) reflectometry to analytically prescribed turbulent plasmas in simplified slab geometry is studied by performing 2D simulations in conventional set-up (i.e. perpendicular incidence) for both cases of poloidal and radial plasma flows. Fixed frequency probing is employed and the reflectometry complex amplitude $A(t)e^{i\varphi(t)}$, phase $\varphi(t)$ and amplitude $A(t)$ signals are characterized while scanning the plasma turbulence level.

II. BRAGG BACKSCATTERING

The most efficient scattering process of the probing wave is caused by density fluctuations that meet the Bragg resonant rule[2-4]. For conventional reflectometry, Bragg backscattering can occur when the local radial wavenumber of the injected wave $k(\boldsymbol{r})$ is resonant with the radial wavenumber of a given Fourier component of the density fluctuations: $k_{rad} = 2k(\boldsymbol{r})$. The Bragg relation holds up to the limit wavenumber $k_{rad} = 2k_o$ set by the vacuum wavenumber of the probing wave k_o, near the plasma entrance. Moreover, only fluctuations with $k_{rad} > 2k_A$ can satisfy the Bragg condition, where k_A is the Airy wavenumber $k_A = 0.63(k_o^2 L_n^{-1})^{1/3}$ with L_n being the density gradient scale length. While the poloidal characteristics of turbulence should not be responsible for any backscattering, in 2D it is impossible to neglect the radiation pattern of the emitter which contains poloidal wavenumbers and could thus resonate with poloidal fluctuations. In the case of O-mode probing and small coherent perturbations in a linear radial profile, a linear relation between the phase perturbations of the reflectometer signal $\delta\varphi$ and the density perturbation amplitude δn has been shown[5,6]:

$$\delta\varphi = \sqrt{\pi} k_o \sqrt{\frac{L_n}{k_f}} \frac{\delta n}{n_c}. \quad (1)$$

where n_c is the cut-off density and k_f a given wavenumber component of the density fluctuation spectrum. However, additional non-linear contributions to phase variations may occur due to higher orders of Bragg backscattering[7].

III. TURBULENCE MODEL

For O-mode propagation, the plasma cut-off for a given probing wavenumber k_o depends only on the plasma electron density n_e. Thus, a numerical plasma is sufficiently modeled by the definition of the electron density. In this work, the total density $n_e(\boldsymbol{r},t) = n_{eo}(\boldsymbol{r},t) + \delta n_e(\boldsymbol{r},t)$ accounts for a linear radial electron density profile $n_{eo}(\boldsymbol{r},t)$ and a broadband density turbulence term $\delta n_e(\boldsymbol{r},t)$. While the background profile is simply set through a given density

[a)]Published as part of the Proceedings of the 22nd Topical Conference on High-Temperature Plasma Diagnostics (HTPD 2018) in San Diego, California, USA.
[b)]Author to whom correspondence should be addressed: jvicente@ipfn.tecnico.ulisboa.pt

gradient, the turbulence is defined by a sum of modes with random phase[8-9]:

$$\delta n_e = \sum_{i=i_m}^{i_M} \sum_{j=j_m}^{j_M} A(i,j)\cos\left[k_x(i)x + k_y(j)y + \varphi(i,j)\right]. \quad (2)$$

The coefficients $A(i,j)$ allow establishing a Kolgomorov-like amplitude k-spectrum, which is in line with several experimental observations in the edge fusion plasmas[10], while $\varphi(i,j)$ is a random generated phase that sets a particular turbulence *snapshot* with the target spectral conditions. The 2D k-spectrum is defined by constant amplitude at low k and up to a chosen wavenumber k_{knee} followed by a power law decay $k^{-\alpha}$ along both the x- and y-directions, corresponding to the radial and poloidal directions in a tokamak. The wavenumber *knee* is set to $k_{\text{knee}} = 400\text{rad/m}$, or $k_{\text{knee}} = 4\text{cm}^{-1}$ in usual (perhaps misleading) notation. The amplitude rolls off dropping to 1% of the flat top value at $k = 15\text{cm}^{-1}$, along with a spectral index $\alpha=3$.

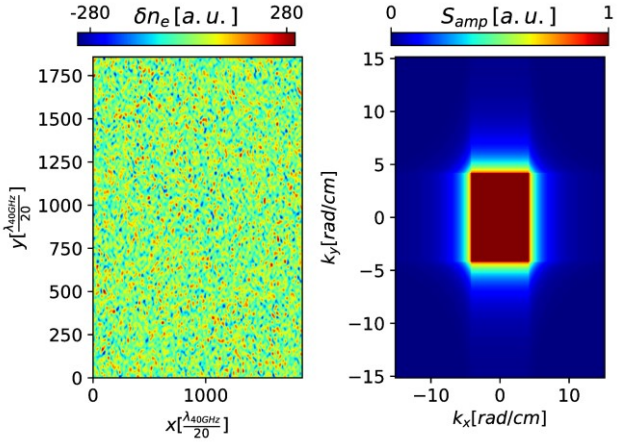

FIG. 1. Example of a 2D density turbulence realization (left) generated with a Kolgomorov-like model of given amplitude k-spectrum (right).

The Root Mean Square value $\delta n_{e,RMS}$ of the density fluctuations generated with the above model, can be easily modified and sets the turbulence level at the radial position r_c of the cut-off density in the slab linear profile:

$$\frac{\delta n_e}{n_e} \equiv \frac{\delta n_{e,RMS}}{n_e(r_c)} \times 100\% \,. \quad (3)$$

The total density, obtained by adding the linear profile and the turbulent density terms, results in a radial variation of the local turbulence level, which increases towards the periphery of the plasma as the background density decreases (see Fig.2). This radial trend is also in general agreement with the experimental observations at the edge and SOL regions of tokamaks[11]. In this work, two different electron density gradient lengths L_n have been used for background profiles, corresponding to shallow (long $L_n \approx 0.16$m) and steep (short $L_n \approx 0.05$m) density profiles, for which the minimum Bragg wavenumbers ($2k_A$) are 1.8cm^{-1} and 2.6cm^{-1}, respectively. Once a total density matrix was generated, simulations were carried out imposing a bulk plasma movement in either the poloidal or radial direction. In both cases, the Taylor "frozen turbulence" hypothesis[12] is assumed, which considers that advection contribution by turbulent eddies is small and that therefore the advection past a fixed point can be taken to be entirely due to the mean flow. This hypothesis actually holds if the eddy mutation rate is much smaller than the mean plasma velocity.

IV. SIMULATION SET-UP

The full-wave code REFMUL used in this work solves the Maxwell equations for O-mode[13]. Both electric and magnetic fields are coupled to the plasma electron density $n_e(\boldsymbol{r},t)$ which is used as fusion plasma model, as mentioned in the previous section. Simulations were designed with a monostatic setup, i.e. one antenna for both emission and reception. A unidirectional transparent source was used for injection of the signal allowing separating the emitted probing wave from any returning waves. For directivity a monostatic 2D H-plane horn antenna with a half-power beam width $\leq$ 6.5cm at the plasma entry was employed. Probing waves with two different frequencies f_p=33GHz and f_p =49GHz, corresponding to cut-off densities of $n_{c33} = 1.35\times10^{19}\text{m}^{-3}$ and $n_{c49} = 2.99\times10^{19}\text{m}^{-3}$, respectively, were used in separate runs. The two slab plasma profiles with the radial cut-off locations of the two probing frequencies that were used are shown in Fig. 2. Also shown are the several turbulence level profiles that were employed in both radial and poloidal plasma flow simulations.

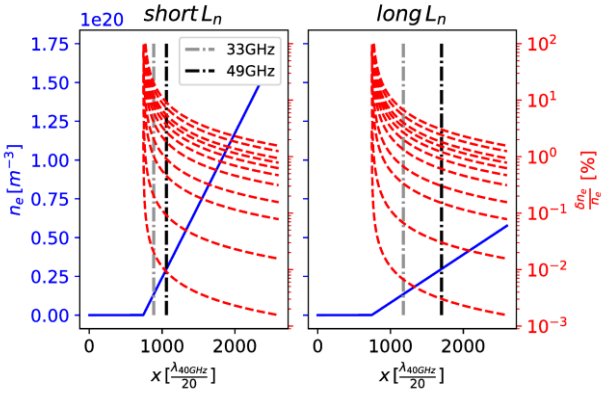

FIG. 2. Linear background density profiles (solid blue) and radial positions of the f_p=33GHz and f_p=49GHz cut-offs, together with the set of density turbulence level profiles (dashed red) employed for the numerical plasmas.

The synthetic reflectometry phase $\varphi(t)$ and amplitude $A(t)$ signals were obtained by performing identical simulation runs with sin and cos excitation signals allowing in-phase $I(t) = A(t)\cos(\varphi(t))$ and quadrature $Q(t) = A(t)\sin(\varphi(t))$ detection. These signals combined provide directly $A(t) = [I(t)^2+Q(t)^2]^{1/2}$ and $\varphi(t) = \text{atan}[Q(t)/I(t)]$. The simulation box comprised a rectangular grid while the plasma itself was quadrangular with side length L =1859 grid points, since a radial block of the simulation box was used for the antenna setup and a vacuum distance (d_{vac} = 15.5cm) to the plasma. The spatial grid resolution was $\Delta x = \Delta y = \lambda_{40\text{GHz}}/20 = 3.75\times10^{-4}$m, where $\lambda_{40\text{GHz}}$ is the vacuum wavelength of a

f=40GHz wave frequency. The required time resolution of the simulations ($\Delta t = 6.25\times10^{-13}$s) impose that the duration of any simulated phenomena must be scaled down and any velocities involved scaled up. A rescaling is done such that $v_{siml} = R_t v_{real}$ where v_{real} is the characteristic velocity of a given plasma feature and v_{siml} the velocity in the simulation. To avoid relativistic effects, the scaled-up velocities v_{siml} are restricted to values of $v_{siml} < 0.1c$, where c is the speed of light. In this work, simulations of plasma propagation in both radial and poloidal directions have been performed with 28×10^4 time iterations, corresponding to $v_{siml} = 0.013c$.

V. SIMULATION RESULTS

A. Poloidal plasma flow

Independent simulations were performed for each turbulence level, in a range of 0.02%-20%. The power spectra of the reflectometry complex amplitude signal $A(t)e^{i\varphi(t)}$ for the unperturbed profile case and a set of turbulence levels are shown in Fig. 3, for each density gradient length and probing frequency that were studied.

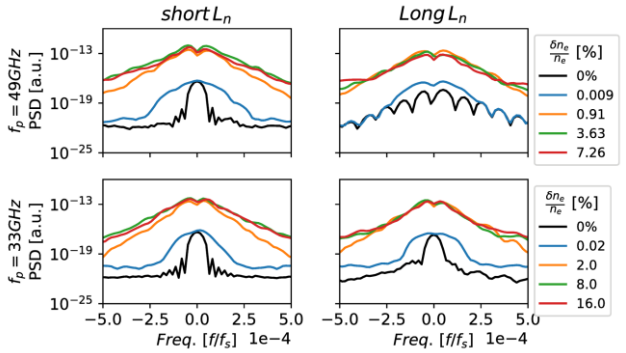

FIG. 3. Power spectra of complex amplitude signals $A(t)e^{i\varphi(t)}$ for turbulence level scans, in two different density gradient lengths L_n and two probing frequencies f_p. Turbulence was generated using a Kolgomorov-like model and set to flow in the poloidal direction.

In general, spectral broadening is observed with increasing turbulence level. The usual increase of central peak amplitudes and integrated spectral powers (see also Fig. 4) with increasing turbulence level is also observed. Similar results were obtained previously with simple physical optics model[8]. It is known that fluctuations moving in the poloidal direction, acting as a phase grating, may result in frequency shifted sidebands at the receiver antenna[14]. The amplitudes of those sidebands are expected to be equal in conventional reflectometry, at least for geometrically symmetric perturbations and low propagation velocities. On the other hand, the poloidal propagation of density structures results in radial displacements of the cut-off layer as the 2D structures project different radial profiles in a perpendicular line of sight. Thus, any radial movements of the reflecting layer should lead to a phase modulation of the reflected signal, resulting in a symmetric broadening of the central line in the frequency spectrum. After rescaling the frequency axis, according to the ratio of velocities, assuming v_{real}=5km/s and taking into account that the frequency of the density fluctuations is related to the poloidal (or equivalently in this case, perpendicular) wavenumber $v_{pol}k_{pol}=2\pi f$, the wavenumber spectra can be reconstructed. This is shown in Fig. 4 for one probing frequency and a comprehensive set of turbulence levels.

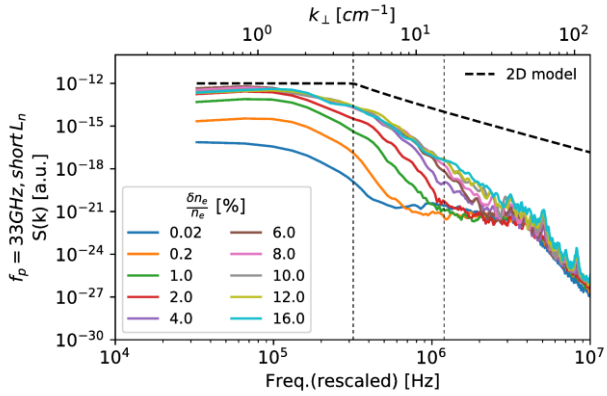

FIG. 4. Power spectra of $A(t)e^{i\varphi(t)}$ signals on re-scaled single-sided frequency axis and corresponding $k_\perp$-axis, for a turbulence level scan with probing frequency f_p=33GHz and short density gradient scale length L_n.

The spectral shape of the input Kolgomorov-like amplitude k-spectrum (shown in dashed line) is fairly well recovered. The flat amplitude region at low-k followed by a strong roll-off region is observed. The values from the original model $k_{knee} = 4\text{cm}^{-1}$ and $k = 15\text{cm}^{-1}$ (1% of the flat top value) are also shown in Fig. 4 by vertical dashed lines. Applying an identical spectral analysis and re-scaling procedure to $\varphi(t)$ and $A(t)$, followed by linear fitting the data in the roll-off region ($4\text{cm}^{-1} < k_\perp < 15\text{cm}^{-1}$) allows obtaining estimates of the spectral index which are shown in Fig. 5.

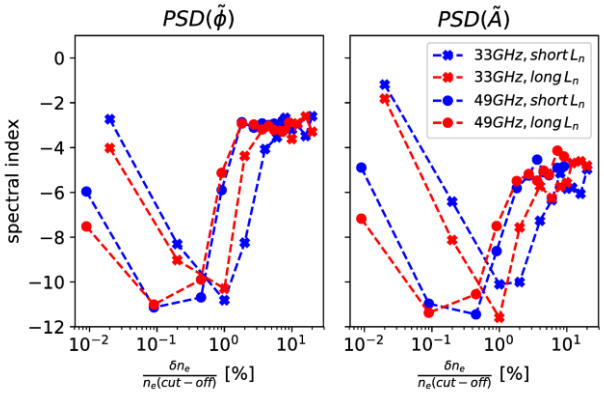

FIG. 5. Spectral index obtained from the fluctuating components of $A(t)$ and $\varphi(t)$ signals in turbulence levels scans with 2 probing frequencies f_p and 2 density gradient scale lengths L_n.

At low turbulence levels the spectral index is mostly under-estimated. However, for $\delta n_e/n_e > 2$-4% the phase spectra do allow to recover the spectral index value (-3) of the 2D model, suggesting that the sensitivity to high k fluctuations may increase at higher turbulence levels or that simply 2D effects farther from the cut-off become increasingly more important. On the other hand, the evolution of the integrated spectral power of the $A(t)e^{i\varphi(t)}$ signals with the turbulence

level, displayed in Fig. 6, shows a linear relation between these two quantities only up to $\delta n_e/n_e \approx$ 2-4% followed by non-linear behavior at higher turbulence levels.

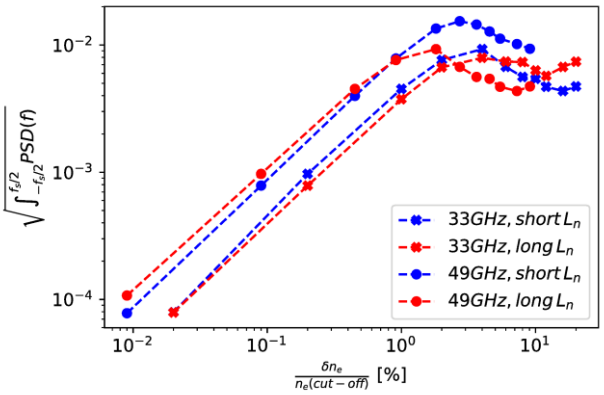

FIG. 6. Root Mean Square (total integrated power spectra) of $A(t)e^{i\varphi(t)}$ signals for turbulence level scans with 2 probing frequencies f_p and 2 density gradient scale lengths L_n.

A similar relation is also observed between the phase fluctuations and the turbulence level, as shown in Fig. 7. In this case, and again only for low turbulence levels, the fluctuating component of the reconstructed phase signals also scales with both k_o and $\sqrt{L_n}$ as prescribed by Eq. (1).

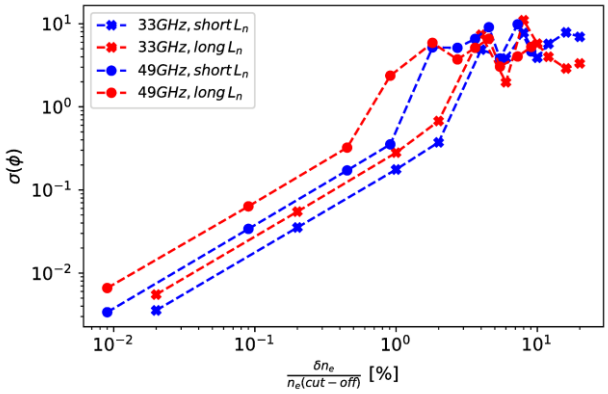

FIG. 7. Standard deviation of reflectometry $\varphi(t)$ signals for turbulence level scans with 2 probing frequencies f_p and 2 density gradient scale lengths L_n.

Starting at moderate turbulence levels, the phase time traces (not shown here) display phase drifting and phase runaway effects that become ubiquitous at higher turbulence levels. The evolution of the average and fluctuating components of the reflectometry amplitude $A(t)$ is shown in Fig. 8. The average amplitude of the reflected signal decreases with increasing turbulence level and is lower, at each turbulence level, in the case of higher L_n. These results must be interpreted in the light of 2D effects since 1D backscattering efficiency is proportional to $\sqrt{L_n}$ however, the beam spreading associated to a longer path into the turbulent plasma should provide a competing geometrical effect[15]. A rebound in the average amplitude is also observed at the highest turbulence levels. This could be explained by a transition to a secondary cut-off, from the slab plasma to a high amplitude density front. While the low turbulence range of linear reflectometry phase response has been previously predicted with 1D analytical reasoning[16], 2D physical optics[17,18] and full-wave models[18], these results suggest a possible extension to measuring capabilities, for instance through proper modelling of the amplitude signals.

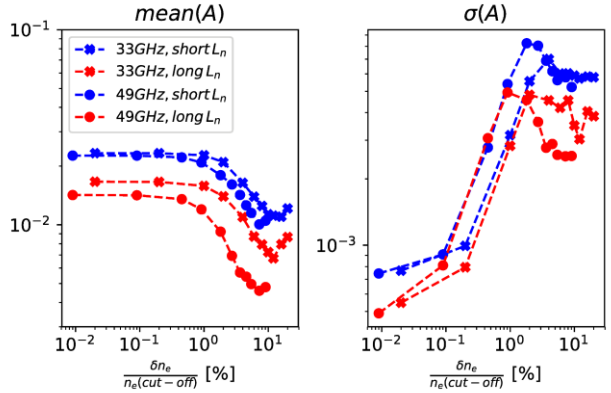

FIG. 8. Average and standard deviation of reflectometry amplitude $A(t)$ signals for turbulence level scans with 2 probing frequencies f_p and 2 density gradient scale lengths L_n.

B. Radial plasma flow

Numerical plasmas employed in the previous section were also used in simulations with radial plasma flow in both inward (V_r >0) and outward (V_r <0) directions. The double-sided Fourier spectra of the complex amplitude signals obtained with the f_p=33GHz cases are shown in Fig. 9.

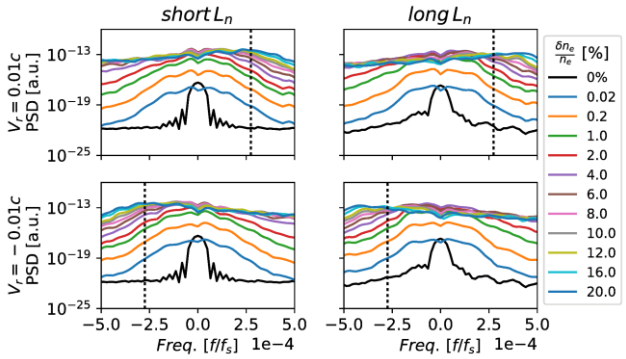

FIG. 9. Power spectra of reflectometry complex amplitude signals $A(t)e^{i\varphi(t)}$ for turbulence level scans in both inward and outwards radial plasma flow directions, with f_p=33GHz probing frequency, and two different density gradient lengths L_n of background *slab* plasmas.

The effect of spectral broadening with increasing turbulence levels is observed again. This is more pronounced than in the poloidal flow cases, shown previously in Fig. 3. The spectra become increasingly asymmetric with increasing turbulence levels. The radial flow can induce Doppler effects at both the cut-off and at Bragg backscattering locations. A single sideband can thus be produced by a density fluctuation with $k_{rad} = 2k(\boldsymbol{r})$ propagating radially. The maximum Doppler shifts expected by the imposed radial velocity on the cut-off layer are shown in Fig. 9 by dashed vertical lines. In cases of short L_n, the observed Doppler shift is in agreement with the reflecting layer movement. For long L_n, the Doppler shifts are larger due to the increased plasma path and Bragg contributions. This is

additionally leading to phase runaway, as seen in Fig. 10 where the phase also changes sign with opposite propagation directions.

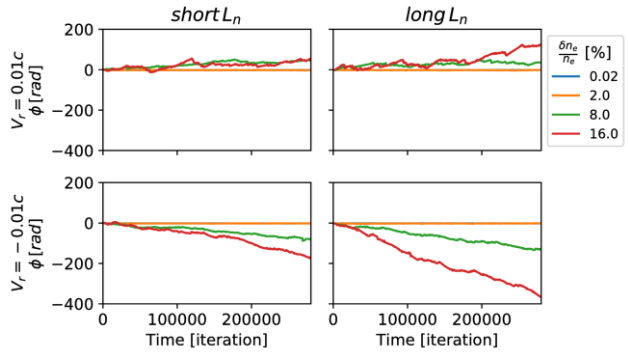

FIG. 10. Time traces of reflectometry $\varphi(t)$ signals for turbulence level scans with f_p=33GHz probing frequency and 2 density gradient scales L_n for both cases of inward and outward radial plasma flow.

Despite this, phase fluctuations behave similarly for the inward and outward directions at low turbulence levels, becoming somewhat distinct at high $\delta n_e/n_e$ possibly due to trapped waves responding differently when being *pushed* out or into the probing wave. For low $\delta n_e/n_e$ values, phase fluctuations scale linearly as predicted by Eq. (1) and shown in Fig. 11 where an average (effective) k_f=3cm^{-1} was assumed to calculate the theoretical Bragg Backscattering values, for two of the outward propagation cases.

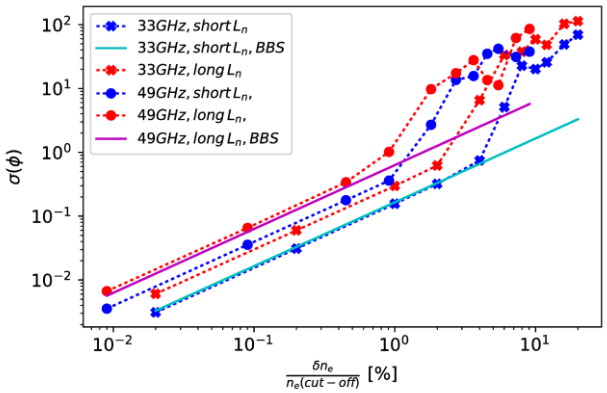

FIG. 11. Standard deviation of reflectometry $\varphi(t)$ signals for turbulence level scans with 2 probing frequencies f_p and 2 density gradient scale lengths L_n, for outward radial plasma flows. Theoretical values estimated from Eq. (1) for two of the simulated cases, are also shown in solid lines.

Standard deviation values $\sigma\varphi(t)$ largely exceeding 2π are perhaps a good proxy for the phase drift slope rather than the phase fluctuations. Nevertheless, this quantity seems to be useful in tracking (quasi-linearly) the turbulence level. The reduction in the average amplitude with both increasing turbulence levels and density gradient length is also observed again, as displayed in Fig. 12. Nevertheless, it is arguable for both $A(t)$ and $\varphi(t)$ fluctuations (and for radial and poloidal plasma flow cases for that matter) if non-linear or saturation regimes are reached at high $\delta n_e/n_e$. Further simulations, extending the turbulence level range, are planned to clarify this behavior.

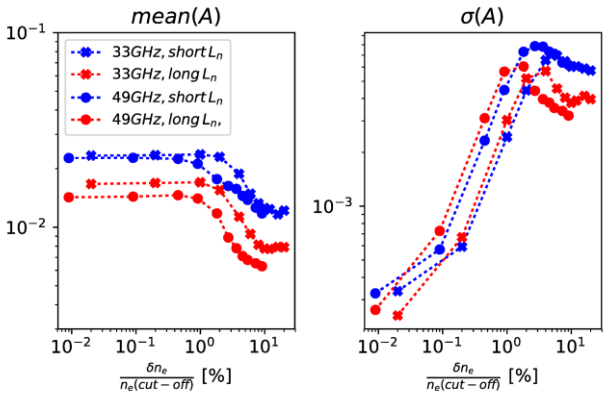

FIG. 12. Average and standard deviation of the reflectometry amplitude $A(t)$ signals for turbulence level scans in the case of outward radial plasma flow for 2 probing frequencies f_p and 2 density gradient scale lengths L_n.

Also, simulations with plasmas obtained from the output of gyro-fluid or gyro-kinetic turbulence codes are ongoing, to have more realistic plasma models, which can then be benchmarked against the results presented here.

VI. ACKNOWLEDGMENTS

This work has been carried out within the framework of the EUROfusion Consortium and has received funding from the Euratom research and training programme 2014-2018 under grant agreement No 633053. The views and opinions expressed herein do not necessarily reflect those of the European Commission. IST activities also received financial support from "Fundação para a Ciência e Tecnologia" through project UID/FIS/50010/2013.

VII. REFERENCES

[1]F. da Silva, S. Heuraux, E. Gusakov and A. Popov, IEEE Trans. Plasma Sci. **38**, 2144 (2010)
[2]N. Bretz, Physics of Fluids B: Plasma Physics **4**, 2414 (1992)
[3]I.H. Hutchinson, Plasma Phys. Control. Fusion **34**, 1225 (1992)
[4]X.L. Zou, L. Laurent and J.M. Rax, Plasma Phys. Control. Fusion **33**, 903 (1991)
[5]C. Fanack *et al*, Plasma Phys. Control. Fusion **38**, 1915 (1996)
[6]B.B. Afeyan *et al.,* Plasma Phys. Control. Fusion **37**, 315 (1995)
[7]I. Boucher *et al.*, Plasma Phys. Control. Fusion **40**, 1489 (1998)
[8]G.D. Conway, L. Schott and A. Hirose, Rev. Sci. Instrum. **67**, 3861 (1996)
[9]S. Heuraux *et al.*, Rev. Sci. Instrum. **74**, 1501 (2003)
[10]M.A. Pedrosa *et al*, Phys. Rev. Lett. **82**, 3621 (1999)
[11]S.J. Zweben *et al*, Plasma Phys. Control. Fusion **49**, S1 (2007)
[12]G. I. Taylor, Proc. R. Soc. A **164**, 15 (1938)
[13]F. da Silva, S. Heuraux, S. Hacquin and M.E. Manso, Journal of Comp. Physics **203**, 467 (2005)
[14]E. Holzhauer, M. Hirsch, T. Grossmann, B. Brañas and F. Serra, Plasma Phys. Control. Fusion **40**, 1869 (1998)
[15]E.V. Sysoeva, E. Gusakov and S. Heuraux, Plasma Phys. Control. Fusion **55**, 115001 (2013)
[16]E. Gusakov, S. Heuraux and A. Yu Popov, Plasma Phys. Control. Fusion **51**, 065018 (2009)
[17]G.D. Conway, Plasma Phys. Control. Fusion **41**, 65 (1999)
[18]J.R. Pinzón, T. Happel, E. Blanco, G.D. Conway, T. Estrada and U. Stroth, Plasma Phys. Control. Fusion **59**, 035005 (2017)